

## DIRECT SIMULATION OF MHD INSTABILITIES IN ALUMINUM REDUCTION CELLS

*D. Munger, A. Vincent*

*Département de Physique, Université de Montréal,  
 C.P. 6128, succ. centre-ville, Montréal (Québec), H3C 3J7, Canada*

**Introduction.** Magneto-hydrodynamic (MHD) instabilities in aluminum reduction cells (see Fig. 1) have been the subject of several studies, since the pioneering work of Urata *et al.* [1]. The interaction between the electrolysis current in the cell and the background magnetic field due to remote currents gives rise to a strong magnetic force acting on the fluids inside the cell. Different kinds of waves thus appear at the interface between a liquid aluminum layer and an electrolytic bath lying on its top. These disturb the current distribution inside the cell so that certain modes become unstable.

It has been shown by means of linear analysis [2, 3] that the longest waves tend to be more unstable, and that resonance may occur between waves propagating along perpendicular horizontal directions and coupled together by the magnetic force. On the other hand, numerical simulations were performed either with industrial codes [4] or a research code using finite elements [5]. These authors mainly focused on obtaining the well-known metal pad roll, a particular instability of which manifests itself as a rotating wave at the aluminum–electrolyte interface.

In order to solve the non-stationary magneto-hydrodynamic equations in a three-dimensional two-fluid system such as the aluminum reduction cell, we have designed a novel numerical method by combining a level set technique together with a finite volumes discretization. Moreover, our equations are written in terms of the magnetic vector potential, thus ensuring the magnetic field to remain exactly divergence-free.

Not only we found, as was done already by [4, 5], that the metal pad roll becomes unstable for some critical value of the background vertical magnetic field but we also simulated a different configuration which resulted in a vertical jet of aluminum. These new results are backed up by a physical explanation of the instability mechanism.

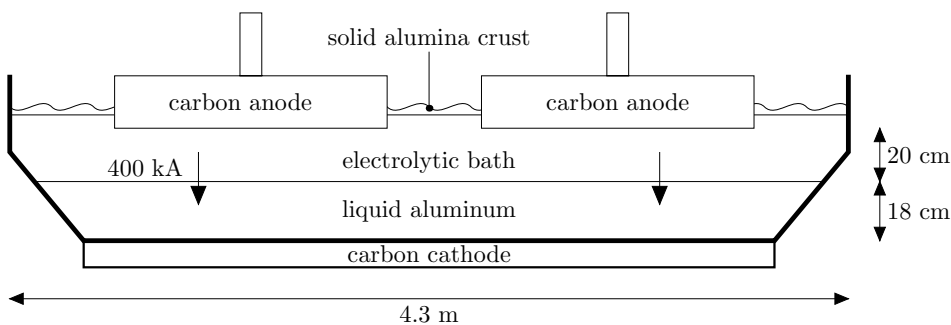


*Fig. 1.* Approximate side view of an AP30 Hall-Héroult cell. The hidden dimension is about 13.6 m deep.

**1. Physical model.** For the sake of simplicity, the system is idealized by considering a single anode spanning over the top of the cell, and by approximating the bottom of the cell to be rectangular. These geometric irregularities are believed not to influence the essential physics of the flow.

*1.1. Conservation equations.* The flow in the cell is described by the unsteady dissipative MHD equations [6]

$$\frac{\partial \mathbf{B}}{\partial t} = \nabla \times \left( \mathbf{u} \times \mathbf{B} - \frac{1}{\text{Lu}} \nabla \times \mathbf{B} \right) \quad (1)$$

and

$$\frac{\partial \rho}{\partial t} \mathbf{u} = -\nabla p - \frac{1}{\text{Fr}^2 \text{Al}^2} (\rho - \rho_0) - \nabla \cdot \left( \rho \mathbf{u} \mathbf{u} - \frac{2}{\text{Re Al}} \mathbf{D} \right) + \mathbf{f},$$

where  $\rho_0$  is the dimensionless density profile at equilibrium (when the aluminum–electrolyte interface is flat and there is no fluid motion),  $\mathbf{D}$  is the usual deformation rate tensor and  $\mathbf{f}$  is the magnetic force. The scaling is based on a unitary interaction parameter or Stuart number (ratio of the magnetic to inertial forces), choosing the height of the cell as the length scale and the electrolyte’s density as the reference mass density. Aluminum is 8.6 % more dense than the latter, so  $|\rho - \rho_0| < 0.086$ . Since the electromagnetics mostly depend on the electrolysis current of magnitude  $J_0$ , we set  $J_0$  as the electric current unit, and  $\mu_0 J_0 L$  as the magnetic field unit. The corresponding dimensionless numbers are the Froude number  $\text{Fr} \simeq 0.18$ , the Alfvén number  $\text{Al} \simeq 0.64$ , and the effective hydrodynamic Reynolds number  $\text{Re} \simeq 76$ , which indeed consists in a zeroth order approximation of the turbulent diffusion of momentum. The Lundqvist number is fluid-dependent and ranges from  $9 \times 10^{-2}$  in the aluminum to  $10^4$  times smaller in the electrolytic bath. For the numerical simulations, the jump is restricted to a  $10^2$  ratio for stability/cost considerations. Note, however, that this is almost physically equivalent, since the bath can be considered as a perfect insulator with contrast to the aluminum.

The electric current is dominated by the vertical uniform downward electrolysis current  $\mathbf{J}_0 = -J_0 \mathbf{e}_z$ , perturbed by a deflection  $\mathbf{j}$  due to: (1) the displacement of the aluminum–electrolyte interface; and (2) the motion of the electrically conducting fluids. The corresponding induced magnetic fields,  $\mathbf{B}_0$  and  $\mathbf{b}$ , respectively, add to a background magnetic field  $\mathbf{B}_{\text{bg}}$  due to remote current sources. These currents are far enough from the system, so it is fair to assume that  $\mathbf{B}_{\text{bg}}$  is uniform or at most linear inside the cell. It is straightforward to show that the force, resulting from the interaction of  $\mathbf{J}_0$  with its self-induced field  $\mathbf{B}_0$ , is irrotational, i.e., will be balanced by a gradient of pressure. Following [7, 8], we constrain  $\mathbf{B}_{\text{bg}}$  accordingly to so such a form that its interaction with  $\mathbf{J}_0$  will give rise to no motion of the fluids. The net magnetic force can therefore be written as  $\mathbf{f} = \mathbf{J}_0 \times \mathbf{b} + \mathbf{j} \times (\mathbf{B}_{\text{bg}} + \mathbf{B}_0 + \mathbf{b})$ .

*1.2. Magnetic potential formulation.* To enforce the divergence-free condition on  $\mathbf{b}$ , the magnetic field is modeled in terms of the magnetic vector potential  $\mathbf{a}$ , uniquely defined by  $\nabla \times \mathbf{a} = \mathbf{b}$  and  $\nabla \cdot \mathbf{a} = 0$  in virtue of Helmholtz’ theorem. Its time evolution is given by:

$$\frac{\partial \mathbf{a}}{\partial t} = -\nabla \varphi + \mathbf{u} \times (\mathbf{B}_{\text{bg}} + \mathbf{B}_0 + \nabla \times \mathbf{a}) + \frac{1}{\text{Lu}} \nabla^2 \mathbf{a} - \left( \frac{1}{\text{Lu}} - \frac{1}{\text{Lu}_0} \right) \mu_0 \mathbf{J}_0, \quad (2)$$

where  $\text{Lu}_0$  is the vertical profile of the equilibrium Lundqvist number. It is straightforward to show that the curl of the latter equation reduces to Eq. (1). The function  $\varphi$  is determined by the gauge condition  $\nabla \cdot \mathbf{a} = 0$ , which allows for a simple, uncoupled diffusion term. While the usual first terms in Eq. (2) may

be self-explanatory, the last one infers from the deflection of the electric current  $\mathbf{j} = -\nabla^2 \mathbf{a}$  due to the displacement of the interface. Taking the laplacian of Eq. (2) shows that the contribution of the last term to  $\mathbf{j}$  is  $\nabla^2(1/Lu)\mathbf{J}_0 - (\mathbf{J}_0 \cdot \nabla)\nabla(1/Lu)$ , which simply depicts the fact that the current tends to flow through the path with the shortest interpolar distance, i.e., the least resistive one. Even though there is a discontinuity in the Lundqvist number at the interface, it makes sense to use gradients of  $Lu$  since, as we will see in Sec. 2.1, a continuous smooth approximation is made.

*1.3. Boundary conditions.* The velocity field is subject to no-slip, no-penetration boundary conditions, so that  $\mathbf{u} = 0$  on the walls. Then, we set no-penetration conditions on the electric current, i.e.,  $\mathbf{j} \cdot \mathbf{e}_n = 0$ , which corresponds to insulating side and bottom walls, together with steady control of the anodic current. This implies  $\nabla^2 \mathbf{a} \cdot \mathbf{e}_n$  on the magnetic potential, but it is straightforward to show that the latter can be obtained by enforcing  $\mathbf{e}_n \cdot \nabla(\mathbf{a} \times \mathbf{e}_n) = \mathbf{e}_n \cdot \mathbf{a} = 0$ , which is much simpler to implement.

## 2. Numerical method.

*2.1. Level set technique.* The motion of the interface is implicitly solved by advecting a scalar level set function  $\phi$ , whose zero-level coincides with the interface [9, 10, 11]. The discontinuities at the interface are smoothed as a function of the distance to the interface. For numerical stability, this smooth transition must span over at least a few grid points. An effective interface width of 2.5 grid points was found to be empirically well suitable for a  $10^2$  conductivity jump ratio.

*2.2. Discretization.* A standard finite volumes spatial discretization with staggered meshes for  $\mathbf{u}$  and  $\mathbf{a}$  [12] allowing for exact projections is used. The averaging–reconstruction cycle is cut down to a less dissipative single reconstruction process thanks to the regular grid.

Time integration is achieved with a second order Adams–Bashforth scheme for all terms but the diffusive ones. The viscous term uses a semi-implicit second order Crank–Nicolson scheme, while the magnetic diffusion term is solved with a fully-implicit backward Euler, due to the very large magnetic diffusion coefficient.

*2.3. Magnetic potential.* Keeping the magnetic field as a divergence-free field is a common problem in numerical MHD. Without an efficient divergence-cleaning method [13, 14], the numerical errors would give rise to artificial “magnetic monopoles” which cause non-physical flow elements to appear [15]. The magnetic potential formulation allows for keeping  $\nabla \cdot \mathbf{b} = 0$  exactly, though it is possible that the gauge condition  $\nabla \cdot \mathbf{a} = 0$  be not satisfied exactly. However, due to the presence of a (physically meaningless) gradient term in Eq. (2), an efficient projection is easily achieved, such that of the velocity field.

## 3. Results.

*3.1. Metal pad roll.* Here, the background magnetic field  $\mathbf{B}_{bg}$  is assumed to be uniform and vertical. As in [4, 5], we obtained the rotating wave known as the metal pad roll [16, 2, 3]. By comparing the periods of these rolling waves for different system sizes, we observed that they correspond to gravity waves, subjected not only to viscous/turbulent damping but also to the net stabilizing effect of the induced currents. The stability threshold was observed to depend on both the intensity of  $\mathbf{B}_{bg}$  and the magnitude of the damping.

*3.2. Vortex pumping.* A gradient of the background magnetic field is now superimposed on the uniform field from the previous section. The gradient in the horizontal component interacts with the vertical imposed current to induce a rotation of the two fluids. The force being equal in both layers with different mass densities, the velocity magnitude becomes higher in the bath than in the aluminum.

The centrifugal pressure discontinuity at the interface infers a curvature to it, which in turn causes a disturbance of the electric currents. These then interact with the vertical component of the background magnetic field to lead to instability. Our numerical simulations show that it takes the form a spinning vertical jet of aluminum.

**4. Conclusion.** Our new, fully three-dimensional numerical method based on a level set technique proved to be successful in reproducing the metal pad roll in aluminum reduction cells, as well as simulating other vortex-based MHD instability. In addition to keeping the magnetic field exactly divergence-free, the vector potential formulation allows for a simple implementation of no-penetration conditions on the electric current disturbance.

#### REFERENCES

1. N. URATA, K. MORI, H. IKEUCHI. Behavior of bath and molten metal in aluminum electrolytic cell. *J. Japan Inst. Light Metals*, vol. 26 (1976), no. 11, pp. 573–583.
2. A. D. SNEYD, A. WANG. Interfacial instability due to MHD mode coupling in aluminium reduction cells. *J. Fluid Mech.*, vol. 263 (1994), pp. 343–359.
3. P. A. DAVIDSON, R. I. LINDSAY. Stability of interfacial waves in aluminium reduction cells. *J. Fluid Mech.*, vol. 362 (1998), pp. 273–295.
4. V. POTOČNIK. Modelling of metal-bath interface waves in Hall–Héroult cells. *Proceedings of the Metallurgical Society of the Canadian Institute of Mining and Metallurgy*, (1989).
5. J.–F. GERBEAU, C. LE BRIS, T. LELIEVRE. Simulations of MHD flows with moving interfaces. *INRIA research report*, vol. 4277 (2001).
6. P. A. DAVIDSON. *An introduction to magnetohydrodynamics* (Cambridge University Press, 2001).
7. A. D. SNEYD. Stability of fluid layers carrying a normal electric current. *J. Fluid Mech.*, vol. 156 (1985), pp. 223–236.
8. A. D. SNEYD. Interfacial instabilities in aluminium reduction cells. *J. Fluid Mech.*, vol. 236 (1992), pp. 111–126.
9. S. OSHER, J. A. SETHIAN. Fronts propagating with curvature-dependent speed: Algorithms based on Hamilton–Jacobi formulations. *J. Comp. Phys.*, vol. 79 (1988), pp. 12–49.
10. M. SUSSMAN, P. SMEREKA, S. OSHER. A levelset approach for computing solutions to incompressible two-phase flow. *J. Comp. Phys.*, vol. 114 (1994), pp. 146–159.
11. M. SUSSMAN, E. FATEMI. An efficient, interface preserving level set re-distancing algorithm and its application to interfacial incompressible fluid flow. *SIAM J. Sci. Comput.*, vol. 20 (1999), no. 4, pp. 1165–1191.
12. J. H. FERZIGER, M. PERIĆ. *Computational Methods for Fluid Dynamics* (Springer–Verlag, 2002), 3rd ed.
13. A. DEDNER, *et al.* Hyperbolic divergence cleaning for the mhd equations. *J. Comput. Phys.*, vol. 175 (2002), pp. 645–673.
14. A. DEDNER, D. KRÖNER, C. ROHDE, M. WESENBERG. Efficient divergence cleaning in three-dimensional mhd simulations. *High Performance Computing in Science and Engineering '02*, edited by E. Krause and W. Jäger, (2003), pp. 323–334.
15. D. MUNGER, A. VINCENT. Numerical simulation of the magnetohydrodynamic instabilities in aluminium reduction cells. In *12th annual conference of the CFD Society of Canada* (Ottawa, Canada, 2004).
16. T. SELE. Instabilities of the metal surface in electrolytic alumina reduction cells. *Metallurgical Transactions B*, vol. 8B (1977), pp. 613–618.